Catalytic Methane Halogenation by Bromine over Microporous SAPO-34 Zeolite Material towards Methyl Bromide, Dibromomethane and Hydrogen Bromide

David Bajec*, Andrii Kostyniuk**, Matej Huš, Matic Grom, Andrej Pohar, Blaž Likozar

Department of Catalysis and Chemical Reaction Engineering, National Institute of Chemistry, Hajdrihova 19, 1001 Ljubljana, Slovenia

Abstract

Background:

Bromination-based methane conversion is one of the promising separate ways of CH_4 valorisation. Both methyl bromide/dibromomethane that are formed can be subsequently transformed into more useful compounds. SAPO-34 could also improve the selectivity (S) towards bromomethane during bromination.

Methods:

To evaluate the performance of SAPO-34 in this reaction process, the influence of time, temperature (T) and weight hourly space velocity (WHSV) rate was investigated in a packed-bed reactor. T was in the range of 310–420 °C, while WHSV was 0.22–1.20 h^{-1}. The molar CH_4 to bromine ratio was 5.4:1. GC-MS was used for analysis of products. Material was characterized by XRD, SEM, NH_3-TPD, N_2 physisorption.

Significant findings:

In the material used for the reaction crystallinity was decreased, solid surface area was reduced, and the density of Brønsted acid sites was also reduced compared to the fresh material. Changes can be attributed to Al_2O_3 loss or also the breakage of Al–O–P bonds, caused by hydrogen bromide ions that are produced. A presence of coke was observed on the zeolite at T higher than 360 °C. CH_2Br_2 decomposes, while CH_3Br is released in intermediate gas phase. Catalytic yield increase compared to homogeneous one was not notable, which indicates on the prevalence of elementary radical mechanism. The highest S for CH_3Br was around 90% at 310 °C with the WHSV of 1.20 h^{-1}.

Keywords: Methane activation, bromination, bromine, SAPO-34, methyl bromide

*Corresponding author
**Corresponding author
Email addresses: david.bajec@ki.si (David Bajec), andrii.kostyniuk@ki.si (Andrii Kostyniuk)

1. Introduction

Natural gas production increased 5% in 2019, one of the largest growth rates in 30 years, and its production is estimated to increase also in the future [1]. Large quantities of natural gas are still being flared and vented [2, 3]. The majority of natural gas that is not wasted is being used for energy purposes (electricity and heating) [4, 5] and for steam reforming [6, 7]. More useful chemicals can be obtained by steam reforming, dry reforming or partial oxidation of methane [8–13] and subsequent Fischer-Tropsch process, but this route is energy demanding and is economical only on a large scale [14]. Several ways of methane conversion to more useful chemicals are being investigated [15]. In direct catalytic valorization of methane there are two distinct approaches. The first one is oxidative methane coupling to C_2 hydrocarbons that proved to be relatively efficient [16], especially with recently developed catalysts that are active at lower temperatures and resistant to sulfur poisoning [17, 18]. The yield of the desired products necessary for industrial use (above 30%) is limited because over-oxidation of methane to CO and CO_2 [16]. The other approach is a non-oxidative one, either by methane dehydroaromatization over Mo/HZSM-5 catalysts [19] or coupling of methane to C_2 hydrocarbons [20–24]. The main problem are thermodynamic limitations of the process, because of difficulties in methane molecule activation [15]. High temperatures, usually above 700 °C, are thus needed to achieve significant conversion of methane [19, 20]. Also deactivation of the catalyst due to coke formation is a significant problem [19].

Instead of oxygen other oxidants can be used for converting methane to more useful chemicals. Such oxidants are sulfur [25, 26] or halogens [27–29]. Methane upgrading via bromination is attractive because it can be accomplished under mild temperatures and with relatively high conversion. Selectivity for one brominated product, for example methyl bromide, can be increased by use of a catalyst. In Figure 1 a possible pathway to obtain ethylene from methane through bromination of methane and subsequent coupling of methyl bromide is shown. Similar approach, by activation with bromine, is used by a company Reaction35, LCC to convert light alkanes into chemicals. Methane bromination can be accomplished in a gas phase and its kinetics was investigated already in 1944 by Kistiakowsky and Van Artsdalen [30]. Gas phase reaction gives a range of bromomethanes. At 525 °C and 1 atm thermodynamic equilibrium for stoichiometric ratio of methane and bromine predicts 39.3% selectivity for bromomethane and 54.1% for dibromomethane, the rest is bromoform. Methane conversion is 59.6%. However, it was observed experimentally that at a longer contact time the product distribution changes in contrast to the thermodynamically predicted one because reproportionation of the products occurs and selectivity for methyl bromide is increased. After reproportionation the selectivity for methyl bromide is 69.5% and the selectivity for dibromomethane is

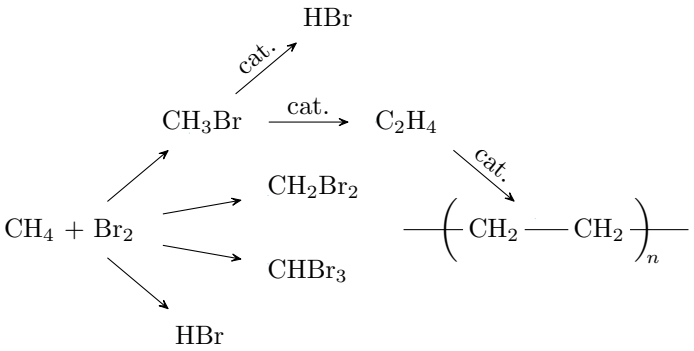

Figure 1: Pathway of methane valorization through bromination of methane and coupling of methyl bromide.

29.5% at 73.5% methane conversion and 525 °C [31]. High yield of methyl bromide is desirable because CH_3Br can be catalytically coupled to ethylene [32, 33] which is in high demand because it is used for the production of polyethylene.

The yield of methyl bromide can be increased further by using different catalysts for methane bromination. Catalytic halogenation of methane was studied by Olah et al. [34, 35]. $SbOF_3/Al_2O_3$ catalyst achieved 99% selectivity for methyl bromide and 20% conversion of CH_4 at 200 °C and gas hourly space velocity (GHSV) of 100 with ratio of Br_2:CH_4 = 0.2 [34]. The same high selectivity of 99% for methyl bromide was achieved by Degirmenci et al. [36] at 340 °C over 25 mol.% zirconia in SBA-15. Conversion of methane was 69% and ratio of Br_2:CH_4 in the feed was approximately 10 with GHSV of 3000 mL/(g·h). Ding et al. [29] have found that addition of iodine catalyses the reaction of bromine with methane in the gas phase and increases the yield of methyl bromide. Argon was used as a carrier gas and the ratio of compounds in the feed mixture was CH_4:Br_2:Ar = 7:7:14 and I_2:Br_2 ratio was 1:9. At 500 °C and reaction time of approximately 31 seconds the conversion of CH_4 was around 70% and selectivity for methyl bromide was around 63% compared to non-catalysed bromination of methane at the same reaction conditions where conversion of CH_4 was around 65 % and selectivity for methyl bromide was only 50%. It was found that I_2 acts as a catalyst in the reaction between methane and dibromomethane producing methyl bromide and thus increasing the selectivity. A number of different catalysts and different support materials were recently evaluated for chlorination and bromination of methane and their performance was compared to the non-catalysed reactions. Materials such as zeolites, sulfated oxides, supported metal-based oxides and supports itself were tested by Paunović et al. [28]. In the bromination of methane only minor effects of the tested catalysts were observed in the range of applied reaction conditions compared to the gas phase reaction. Batamack et al. [37] reported that at different reaction conditions SAPO-34 can improve the selectivity towards mono halogenated products in the chlorination and bromination of methane. At 365 °C and space velocity of 144 mL/(g·h)

the selectivity for methyl bromide was 100%. The ratio of CH_4/Br_2 was 10.3. At a lower space velocity and at the same temperature higher hydrocabons were forming. At space velocity of 43.2 mL/(g·h) and with 10 g of SAPO-34 the selectivity for methyl bromide was only 36.4% on the account of higher hydrocarbons formation. Neither dibromomethane nor bromoform were detected. Propane accounted for approximately 27 mol.% of the hydrocarbon products, followed by ethylene with 15 mol.% and propylene with about 8 mol.%. The rest of the products were C_4 and C_{5+} hydrocarbons and ethane. Therefore by increasing the residence time methyl bromide was oligomerized to higher hydrocarbons on the SAPO-34. Indeed, it is known that SAPO-34 can catalyse coupling of methyl bromide to ethylene [32, 33].

In this work SAPO-34 was used as a catalyst for bromination of methane. A set of experiments was conducted in a packed-bed reactor in order to investigate the influence of temperature and weight hourly space velocity (WHSV) on the selectivity for methyl bromide and conversion of bromine. Reactivity of dibromomethane over SAPO-34 was also tested. Integrity of the material during the reaction was investigated by characterizing the material before and after the use in methane bromination. Conditions for methane bromination were selected to be in the similar range as in ref. [37], where a hundred percent selectivity for methyl bromide was achieved. A larger range of temperatures was considered (from 310 to 420 °C compared to only 345 and 365 °C in ref. [37]). Also a lower CH_4:Br_2 ratio was used because at higher temperatures greater conversion of bromine was expected. WHSV ranged from 0.22 to 1.20 h^{-1} while in ref. [37] WHSVs of 0.18 and 0.56 h^{-1} were used at 365 °C to achieve a hundred percent selectivity to methyl bromide. In this work the highest selectivity for methyl bromide (above 90%) was achieved at the lowest temperature (310 °C) and WHSV of 1.2 h^{-1} and the largest conversion of bromine (around 70%) and methane was obtained at the highest temperature 420 °C and low WHSV of 0.31 h^{-1} while selectivity to methyl bromide was approximately 90%.

2. Experimental

2.1. Materials

SAPO-34 molecular sieve with SiO_2/Al_2O_3 ratio of 0.5 was purchased from ACS Materials in the protonated form. The material was received pre-calcined at 550 °C. The average size of the particles is specified to be 2 μm. Bromine with purity of ≥99% was purchased from Merck and used as received. Dibromomethane had purity of ≥98.5% and was used without purification (Merck). Methane (grade 3.5) was purchased from Linde. Silicon carbide (purity ≥99.5%) with the particle size range of 180 – 250 μm was purchased from Nanografi Nanotechnology AS.

2.2. Catalyst characterization

X-ray powder diffraction (XRD) measurements were done on PANalytical X'Pert PRO diffractometer with CuKα1 wavelength of 1.540598 Å. The range of the 2θ angle was from 5 to 40 degrees with the resolution of 0.033°. Scanning electron microscopy (SEM) images were taken on Zeiss Supra 35 VP. N_2 physisorption was performed on Micromeritics ASAP 2020. The mass of the sample was approximately 100 mg. At first the sample was evacuated at 300 °C for 2 hours. Thereafter the sample was cooled down and adsorption and desorption of N_2 was performed. Specific surface area was determined by Brunauer-Emmett-Teller (BET) theory [38]. Volume of micropores was calculated by t- plot method [39]. Temperature programmed desorption of ammonia (NH_3-TPD) was accomplished on Micromeritics AutoChem II. The sample (approximately 100 mg) was first treated for 1 hour at 500 °C in He (20 mL/min). After that the sample was cooled down to 50 °C and gas flow was switched to 10 vol.% NH_3 in He and the sample was exposed for 30 min. After that the gas was switched back to carrier gas (He) and the desorption was started by increasing the temperature with a rate of 10 °C/min from 50 to 600 °C. The desorbed NH_3 was detected by mass spectrometer (MS). After desorption was completed the calibration of MS was carried out. Several pulses with known concentration of NH_3 were flushed by carrier gas to the MS while the sample was in bypass.

2.3. Reactions in packed-bed reactor

Catalytic experiments were done in a quartz packed-bed reactor. Temperature of the aluminium block used for heating was controlled by Pixsys atr 243 controller. The length of the isothermal zone in the reactor was 110 mm. The inner diameter of the reactor was 6 mm. The flow rates of gases (methane and nitrogen) were regulated by Brooks mass flow controllers. Nitrogen was used as an internal standard. For methane bromination experiments bromine was introduced into a glass evaporator by a syringe pump (TSE systems model 540060). Methane was flown through the evaporator and methane/bromine gas mixture was led into the reactor. The internal standard line was connected to the reactor outlet. Bromine reacts with stainless steel, therefore all the tubes in contact with bromine were made from polytetrafluoroethylene (PTFE). The evaporator was at room temperature. Experiments were performed at atmospheric pressure and the molar ratio of CH_4:Br_2 was not smaller than 10:2 thus it was ensured that all the bromine that was being pumped into the evaporator was able to evaporate at the same rate. On-line analysis of the products was ensured by a custom made PTFE lined gas sampling valve (purchased from Gasgrom d.o.o.) installed on the inlet of a gas chromatograph (GC, Agilent Technologies GC 7890A). A heated tube was connecting the outlet

of the reactor and the inlet on gas chromatograph equipped with a mass spectrometer detector (Agilent Technologies MSD 5975C). 15 m long Agilent J&W GS-CarbonPLOT column was used for the separation of compounds. The column pressure was constant and it was set to 70 kPa. Temperature programme was set to 45 °C for 2 minutes followed by a temperature ramp (30 °C/min) up to 300 °C. This temperature was then held for long enough time for all the products to elute. The instrument was calibrated for CH_4, CH_3Br and CH_2Br_2. Calibration for methane was done with different concentrations of CH_4 in $CH_4/He/N_2$ mixtures prepared by mass flow controllers and flown through the reactor system. Gas mixtures with different CH_2Br_2 concentrations were prepared by dosing dibromomethane with different flow rates into evaporator by syringe pump and flowing He through the evaporator. For the calibration of CH_3Br gas mixtures with different concentration of CH_3Br in He and N_2 were prepared by dosing the gases into the gas container and weighing it. Bromine was not detected by MS and HBr was not separated on the column and was appearing as an elevated baseline when the GC oven was heated to 300 °C.

For all the experiments (Table 1) 1 g of SAPO-34 was used. The material was first pressed in a hydraulic press, crushed and sieved to particle size in the range of 250 – 400 μm. Then it was put into the quartz reactor. The procedure was as follows. First quartz wool was packed at the bottom of the reactor then silicon carbide chips were put into the reactor to the suitable height for the catalyst to be in the middle of the isothermal zone. After that 1 g of sieved catalyst was put on top of the SiC. The remaining volume on the top of the catalyst was also filled with SiC. The filling of the space above and under the catalyst with SiC helped to minimize the gas phase reaction before and after the catalytic zone. In Figure S1 in Supplementary info an example of the prepared quartz tube containing SiC and the catalyst after the reaction is shown. For all the experiments the CH_4:Br_2 molar ratio was around 5.4:1.

Table 1: Experimental conditions.

WHSV [h^{-1}]	Temperature [°C]
0.22	310, 330, 340, 360, 375, 390
0.31	310, 330, 340, 360, 375, 400, 420
0.60	310, 330, 350, 375
1.20	310, 330, 350, 375

3. Results and discussion

3.1. Catalyst characterization

In Figure 2 the diffractograms of the fresh SAPO-34 and two spent SAPO-34 samples, denoted SA-a and SA-b are shown, respectively. The diffractogram of the fresh catalyst exhibits a characteristic pattern of SAPO-34 with a typical chabazite framework [40]. Sharp peaks show high crystallinity of the commercial SAPO-34 with the average particle size of around 2 µm as reported by the manufacturer. The first spent catalyst (SA-a), was on stream for 30 hours with WHSV of 0.6 h^{-1} in the temperature range of 300–365 °C. The second catalyst, SA-b in Figure 2 was used at higher temperatures in the range from 300 up to 390 °C. The total time on stream for this catalyst was 72 h. For the SA-a sample no coke was observed after the reaction when the catalyst was taken out from the reactor. The colour turned from white prior to the reaction to orange after the reaction. The orange colour was preserved to some extent even after the evacuation of the sample overnight at 10 mbar and 120 °C. The appearance of the material after the evacuation is shown in Figure S2 and photograph of the used catalyst before evacuating is shown in Figure S1, both in Supplementary info. At temperatures equal to 380 °C and higher the material started to coke.

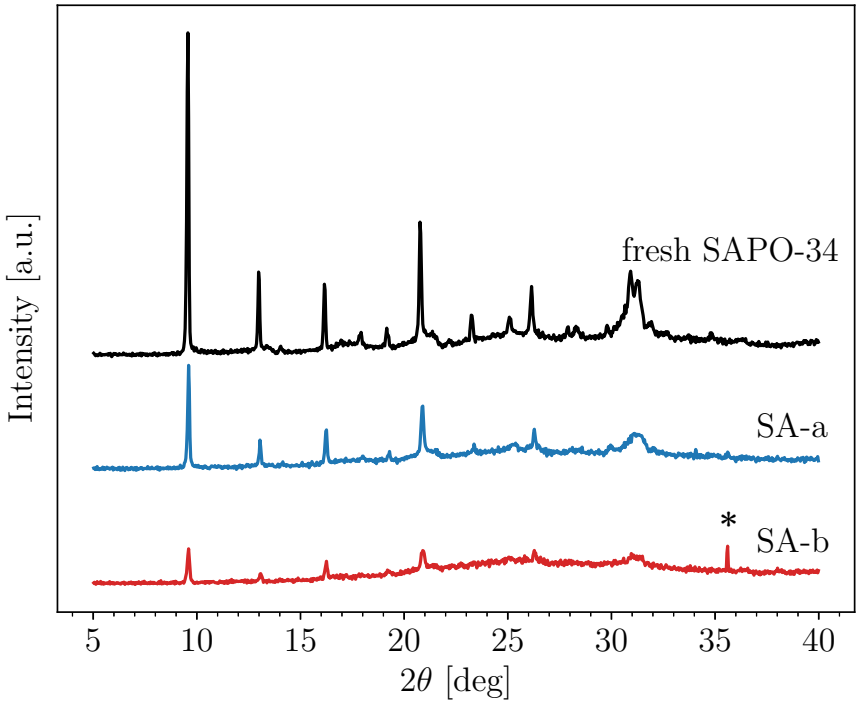

Figure 2: X-ray diffractograms of fresh SAPO-34 and two SAPO-34 samples after the reaction.

The photographs of the coked catalysts are shown in Figure S3 and Figure S4 in Supplementary info. The diffractogram of coked catalyst (SA-b) is shown in Figure 2. Both spent catalysts (SA-a and SA-b) show a decrease in crystallinity as is evident from the decrease in peak height compared to the fresh SAPO-34. Coked catalyst was used in reaction at higher temperatures and for longer time on stream therefore the decrease in crystallinity is more pronounced. The small sharp peak, marked with asterisk at 35.6° is present because a particle of SiC found its way into the sample for the analysis. The peak corresponds to (111) plane of SiC [41]. From the diffractograms it can be seen that the material was apparently changing during the reaction. This is most likely because of damage in SAPO-34 structure caused by Br_2 and by HBr that was forming during the reaction. Paunović et al. [42] studied the influence of HBr, HCl, Cl_2 and Br_2 on structure of HZSM-5. They found that Br_2 and HBr cause dealumination of the zeolite via halogen coordination. The presence of Al–Br bonds was confirmed by Raman spectroscopy and the aluminium redistribution was studied by solid state ^{27}Al MAS NMR. However, no extensive loss of crystallinity was observed upon contacting the zeolite with HBr or Br_2. The material used in this study contained significantly higher amount of aluminium compared to the one used in the work of Paunović et al. [42], since the SiO_2/Al_2O_3 ratio of SAPO-34 used herein was 0.5 (with 42 wt.% Al_2O_3 according to the manufacturer) and the SiO_2/Al_2O_3 ratio of HZSM-5 was 80 [42]. Therefore, it is likely that extensive dealumination in a material with high content of aluminium caused deformation of the regular structure of SAPO-34 and thus a decrease in the crystallinity. The dealumination was most probably caused by HBr that was forming during the reaction, since dealumination is more extensive upon contacting HZSM-5 with hydrogen halides than with halides (Br_2 or Cl_2) [42]. Additionally, Wei et al. [43] reported that HCl can also react with SAPO-34 and cause breakage of Al–O–P bonds. Similar breakage could also occur while SAPO-34 was in contact with HBr causing observed decrease in crystallinity.

Under the scanning electron microscope it can be seen that the zeolite particles were not visibly damaged after the reaction. This is shown in Figure 3, where fresh SAPO-34 (A) and used catalyst sample SA-a (B) are shown. The cracks present in both samples were caused by hydraulic pressing of the material in a hydraulic press prior to crushing and sieving. Regular shaped cubes of SAPO-34 with diameter approximately 2 μm are seen in both SEM images. The samples shown are the same as the samples used for XRD analysis (fresh and used SAPO-34). It is apparent that the dealumination decreased the crystallinity of the used sample but it did not cause destruction or collapse of the particles. On the energy-dispersive X-ray spectroscopy (EDX) mapping in SEM images bromine was detected on the used catalyst as shown in Figure S5 in Supplementary info. This is in agreement with the study on the influence of halogens and hydrogen halides on HZSM-5

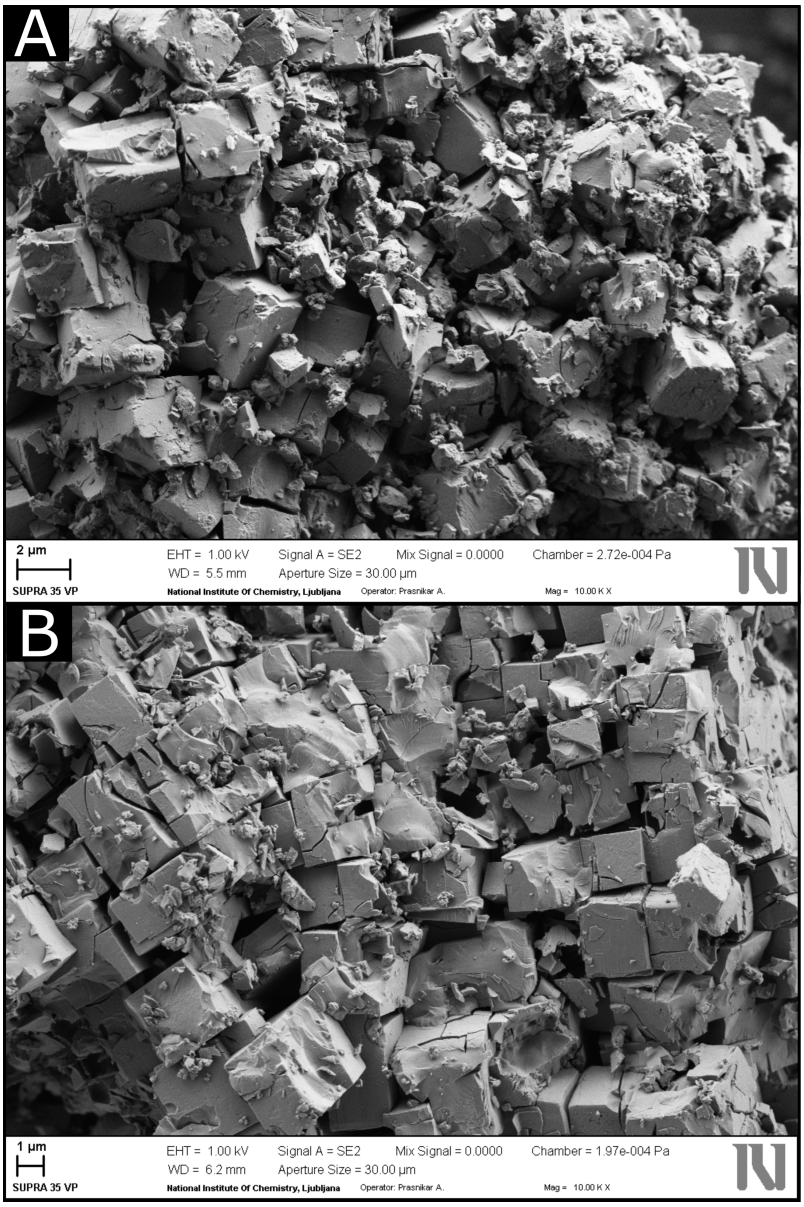

Figure 3: SEM images of fresh (A) and spent SAPO-34, SA-a sample (B). Reaction conditions for SA-a: WHSV = 0.6 h^{-1} , T = 300 – 365 °C, TOS = 30 h.

mentioned before [42], where bromine was observed with EDX in transmission electron microscope on the zeolite after the treatment with HBr or Br_2 at 450 °C for 5 hours. Therefore bromine atoms were incorporated in the framework of SAPO-34 through Al–Br bonds similar to what happens in the case of HZSM-5 and HBr. According to ref. [42] the Brønsted acidity of HZSM-5 decreased after exposure to HBr because of Br incorporation in material and destruction of Al(OH)Si bonds. The concentration of Brønsted acid sites decreased from 167 µmol/g to 87 µmol/g after the zeolite was contacted with HBr at 450 °C for 5 hours.

During the bromination of methane a significant amount of HBr is forming. HBr reacts with the zeolite and can alter its acidity. NH_3-TPD was used for determination of the amount of acid sites. Usually a more suitable technique for determination of amount of Lewis and Brønsted acid sites (BAS) is infrared spectroscopy with pyridine as a probe molecule in acid catalysts but because the kinetic diameter of pyridine molecule (d = 5.7 Å) is larger than the pore size of the SAPO-34 (d = 3.8 Å), which has a chabazite type framework, this was not possible. This issue was recently pointed out by Tian et al. [44] and previously by Wang et al. [45]. The former group used pyridine to determine the amount of acid sites only on the external surface of the catalyst particles. Martins et al. [46] showed that in the case of SAPO-34 it is possible to use fitting of Gaussian curves to NH_3-TPD profile and to extract amounts of three different strengths of BAS from the total acidity. The NH_3-TPD profiles of fresh and used SAPO-34 are shown in Figure 4. The unused material shows two distinct desorption peaks. The entire profile can be fitted by four Gaussian curves. Dashed line represents the sum of the fitted Gaussian curves. Martins et al. [46] studied acid properties of the prepared SAPO-34 with the same SiO_2/Al_2O_3 ratio (0.5) by FTIR and NH_3-TPD techniques. After fitting the profile with Gaussian curves the separate peaks were attributed to different acid sites. The low temperature peak at around 80 °C in NH_3-TPD profile was ascribed to physically adsorbed ammonia, the peak at 160 °C was observed due to the desorption of NH_3 from Lewis acid sites or from the dimers $N_2H_7^+$ which can form by adsorbtion of NH_3 to NH_4^+ that is already adsorbed on Brønsted acid sites (BAS) and the 3 high temperature peaks were ascribed to 3 different BAS.

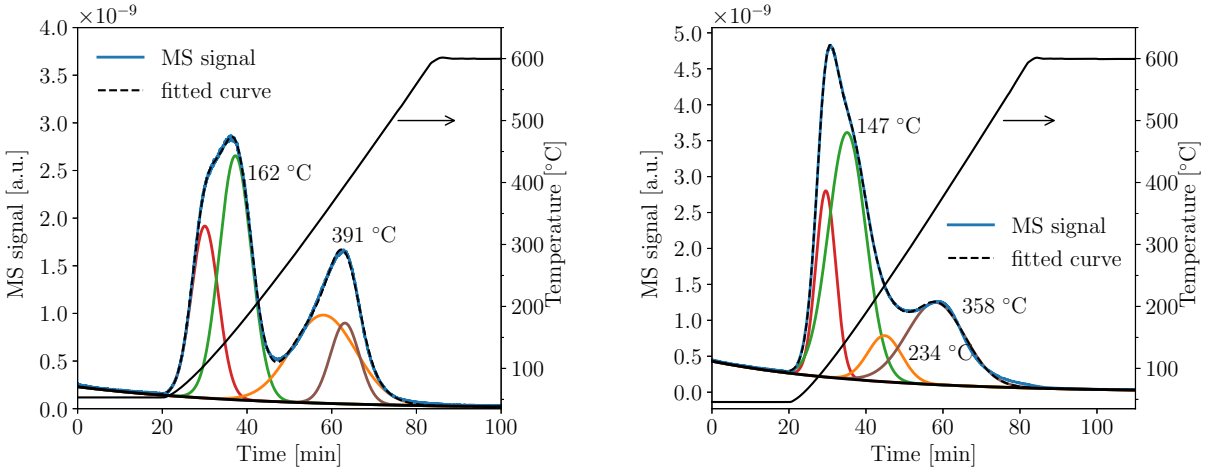

(a) Fresh SAPO-34.

(b) SA-a sample. Reaction conditions: WHSV = 0.6 h^{-1}, T = 300 – 365 °C, TOS = 30 h.

Figure 4: NH_3-TPD curves with peak decomposition by fitting of Gaussian curves.

The first peak for fresh SAPO-34 in Figure 4a is positioned at 104 °C. The temperature ramp with 10 °C/min was started immediately from 50 °C as opposed to the report of Martins et al. [46], where the peak for physisorbed ammonia was observed when the temperature was held constant at 80 °C. Therefore the first peak in Figure 4a is a result of desorption of physically adsorbed NH_3. The second Gaussian peak at 162 °C is observed because of desorption of NH_3 from Lewis acid sites or because of desorption of ammonia bound to ammonium ions on BAS [46]. The composite peak (composed of two Gaussian curves) at 391 °C is observed due to desorption of probe molecules from BAS. The peak position for BAS is similar as in an older study [47], where the same commercial SAPO-34 (ACS materials) was used. In contrast with the work of Martins et al. [46], where three distinct types of BAS were identified, namely OH_a, OH_b, OH_c [46], only two types of BAS are observed after fitting the Gaussian peaks on the TPD profile of fresh SAPO-34. The lower temperature peak of BAS is seen at 347 °C and the peak at a higher temperature is positioned at 395 °C. After the reaction the peak corresponding to desorption of NH_3 from BAS is shifted towards lower temperature namely, from 391 °C to 364 °C (Figure 4b), indicating a decrease in the strength of BAS, possibly due to the changes in the material and formation of OH_c acid sites (peak at 234 °C). The peak corresponding to OH_c was identified exactly at 234 °C by Martins et al. [46]. Again the peak is composed of two peaks positioned at 234 and 358 °C. The peaks for physically adsorbed and weak acid sites remained at approximately the same position as can be seen in Figure S6 in Supplementary info where the overlay of the two profiles is shown with respect to temperature. The intensity of the two signals is not comparable because the measurements were not taken in a narrow time interval and the MS response changed. The values of determined acid site densities are presented in Table 2. Quantitative analysis of the BAS showed that the concentration of BAS in the fresh SAPO-34 is 2.38 mmol/g. This value was calculated from the areas of the two peaks composing the peak at 391 °C. The concentration of Lewis acid sites and ammonia bound to NH_4^+ was 3.68 mmol/g (peak at 162 °C). After the reaction the concentration of BAS decreased. The sample SA-a had 2.0 mmol/g of BAS (areas of peaks at 234 °C and 358 °C). This is similar to what was observed in the case of HZSM-5 after contacting with HBr, where the decrease in BAS was almost 50%. It was shown that this is due to the incorporation of Br in the zeolite lattice [42]. The decrease in concentration is not as large here because the temperature of the reaction for the sample SA-a was lower than in the case of HZSM-5 treatment with HBr. However, the decrease in BAS concentration together with SEM-EDX indicate that Br was indeed incorporated in the SAPO-34 during the reaction and that the decreased crystallinity observed in XRD (Figure 2) was most probably observed due to breakage of Al(OH)Si bonds as suggested by Paunović et al. [42]. Also an increase in the amount of Lewis acid sites indicates that

also some dealumination occurred. In fact, an increase in the peak corresponding to the desorption of NH_3 from Lewis acid sites and from $N_2H_7^+$ dimers was observed. It should be noted that this peak cannot be ascribed unequivocally to Lewis acid sites only and this is not a strong evidence for dealumination and formation of extra-framework aluminium species. However, taking into account all the other evidence it is clear that dealumination did in fact occur. The amount of ammonia desorbed from this peak in the case of fresh SAPO-34 was 2.31 mmol/g and in the case of used SAPO-34 (sample SA-a) this amount was 2.91 mmol/g. The values are presented in Table 2.

Table 2: Results from N_2 adsorption/desorption and NH_3-TPD.

Sample	S_{BET} [m^2/g]	V_{micro} [cm^3/g][a]	LAS [mmol/g]	BAS [mmol/g]
SAPO-34	453.9	0.232	2.31	2.38
SA-a[b]	330.5	0.164	2.91	2.00
SA-b[c]	128.6	0.063	n.d.	n.d.

[a] *t*-plot method, [b] TOS = 30 h and T = 300–365 °C, [c] TOS = 72 h and T = 300–390 °C, n.d. - not determined

The N_2 adsorption/desorption isotherms for SAPO-34 and spent catalysts (sample SA-a and SA-b) are shown in Figure 5. In all three cases type-I isotherms are observed. This type is typical for microporous materials with narrow micropores [48] and for SAPO-34 with no mesoporosity [49]. Apparently, in the used material (SA-a) no additional mesopores were formed since the shape of the adsorption/desorption isotherms is the same as in the fresh material and no hysteresis is observed. Therefore, the bromine that reacted with the material did not cause formation of larger pores that could be detected by this technique, although the crystallinity of the material was decreased (Figure 2) after the bromination of methane over SAPO-34. In the SA-b sample slight hysteresis is observed which might indicate on the presence of some mesopores and on damage in the material. Especially, because it is accompanied with severely decreased crystallinity. The BET surface area of all the samples (330.5 m^2/g for SA-a and 128.6 m^2/g for SA-b) was lower after the reaction than of the fresh SAPO-34 (453.9 m^2/g). Micropore volume, determined by *t*-plot method, also decreased from 0.232 cm^3/g before the reaction to 0.164 cm^3/g after the reaction in sample SA-a and to 0.063 cm^3/g in sample SA-b (Table 2). This is due to pore blockage possibly by aluminium species in the case of SA-a, since the increased peak for lewis acid sites in ammonia TPD indicates on dealumination, and also by coke in the case of SA-b.

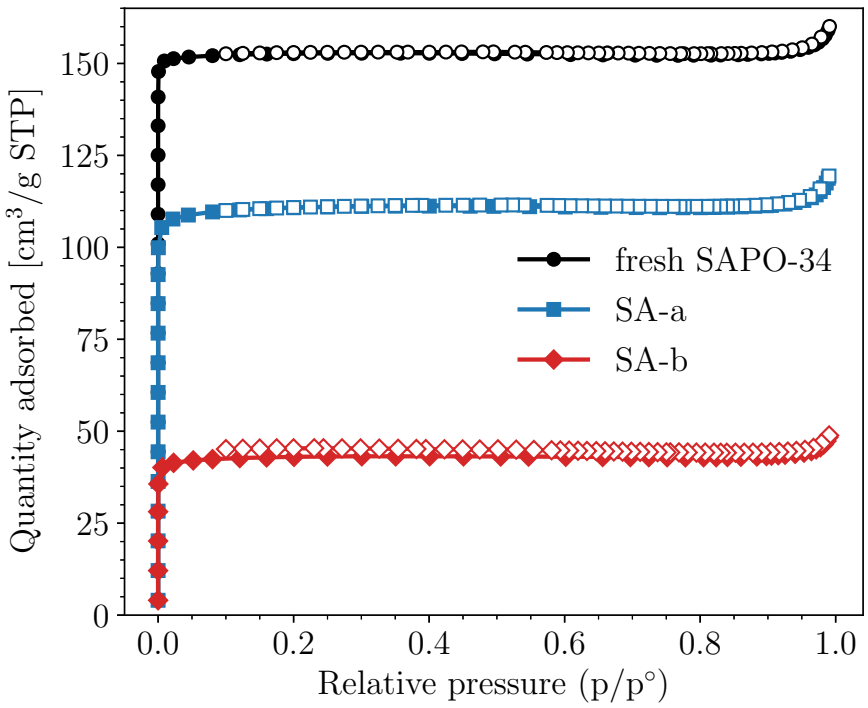

Figure 5: N_2 adsorption/desoprtion isotherms for fresh and used SAPO-34.

3.2. CH_4 bromination reactions

At all the catalytic reactions the only detected products were methyl bromide and dibromomethane. This is shown in Figure S7 in Supplementary info where an example of chromatogram, taken during one of the experiments, is shown. These two products were also detected by Paunović and Pérez-Ramírez [28] when SAPO-34 was used in bromination of methane. The time of the GC method was extended to 26 min to ensure that all the products could elute during the run. The only distinct peaks that can be seen correspond to nitrogen, methane, methyl bromide and dibromomethane. HBr was accumulating on the column and started eluting when temperature was raised causing an increase in the baseline. Both a heightened baseline after 10 minutes and the broad peak between 8 and 10 minutes are result of HBr elution at 300 °C (Figure S7).

In Figure 6 a course of concentrations in one of the experiments for both detected products with time is shown. In this particular experiment the WHSV was 0.31 h^{-1}. The temperature of the reactor was changed stepwise during the time on stream (TOS). After every change the temperature was not changed again until a steady state was achieved. At lower temperature the steady state was achieved almost instantly but at 375 °C a significant delay was observed. Probably the time to reach steady state temperature profile in the

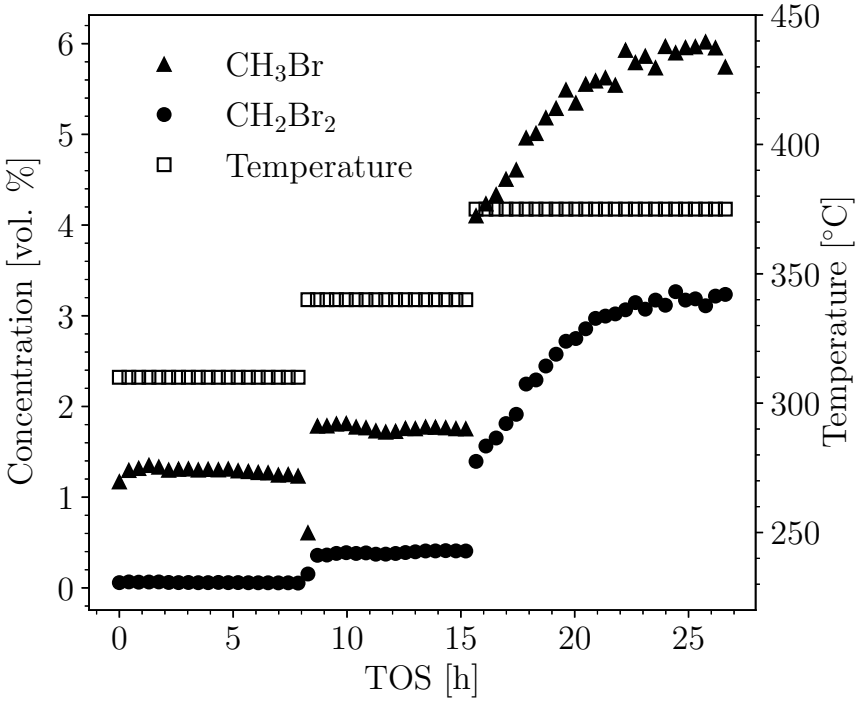

Figure 6: Results of the methane bromination over SAPO-34 at WHSV = 0.31 h^{-1}.

isothermal zone was longer because of a higher set temperature. At this temperature the concentrations of methyl bromide and dibromomethane were 6 vol.% and 3.2 vol.%, respectively. At lower temperatures a much lower concentrations were obtained. The largest increase was when changing temperature from 340 to 375 °C. Namely, at 340 °C approximately 1.8 vol.% of CH_3Br and 0.4 vol.% of CH_2Br_2 were obtained. At 310 °C insignificant amount of CH_2Br_2 was formed and concentration of methyl bromide was around 1.2 vol.%. Concentrations of methyl bromide and dibromomethane obtained at all experimental conditions are presented in Figure 7. Not all experiments were performed at all 9 temperatures and all 4 WHSVs as shown in Table 1. The amount of methyl bromide was increasing with temperature (Figure 7a), for all WHSVs, while the formation of dibromomethane was increasing only up to 375 °C at WHSV 0.22 and 0.31 h^{-1}. At higher temperatures concentration of CH_2Br_2 decreased again (Figure 7b). The maximum concentration of dibromomethane was reached at 375 °C. At temperatures above 375 °C coke began to deposit on the SAPO-34. It is possible that dibromomethane begins to decompose on SAPO-34 at higher temperatures, forming coke which results in a lower dibromomethane concentration. The trend of increasing methyl bromide concentration with temperature was expected as the rate of reactions increases with temperature. From the comparison of methyl bromide concentrations at the same temperatures but different WHSVs, however,

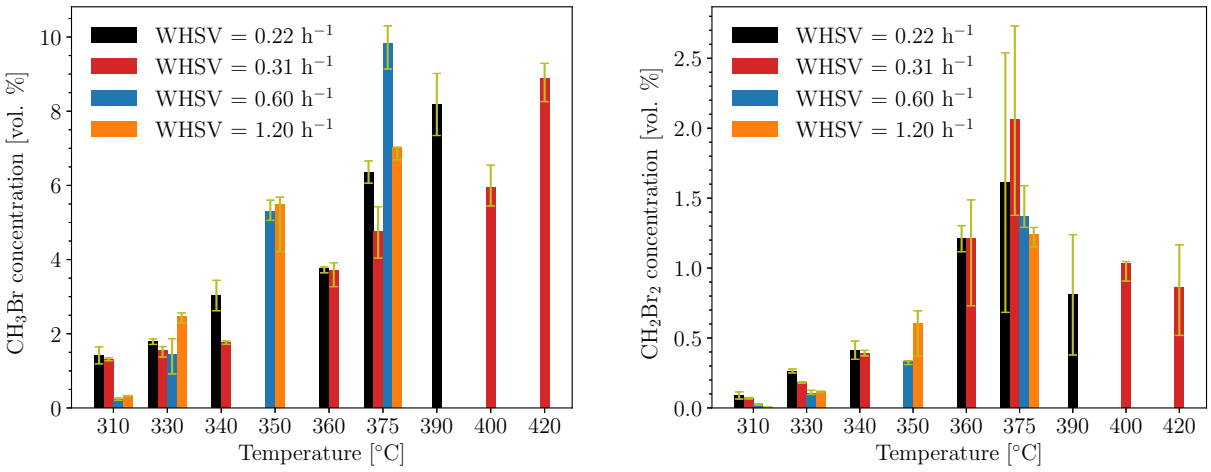

(a) Methyl bromide

(b) Dibromomethane

Figure 7: Concentrations of detected products at different reaction conditions (WHSV and T).

there is no clear trend. At a temperature of 310 °C, the concentration of methyl bromide decreased with WHSV for the first three smallest values of WHSV, but the concentration was again higher at the largest WHSV. A slight decrease of methyl bromide concentration with WHSV was also observed at 340 °C, but at 350 and 360 °C this trend was no longer valid. At 375 °C the declining trend is seen from 0.22 h^{-1} to 0.31 h^{-1} and from 0.6 h^{-1} to 1.2 h^{-1}. Comparing the values of concentration in all four WHSVs there is no trend of decreasing CH_3Br concentration with WHSV. From the results it is also not possible to determine a clear trend of bromine conversion, which should decrease with the increase of WHSV. Given that all the experiments were performed with the same amount of SAPO-34 that was placed in the reactor at the same position and was prior to the experiment treated in the same way, the most probable reason for such deviations is the way the experiments were carried out. Namely, in each experiment after the temperature was changed, it was necessary to wait for reaction to reach a steady state. At lower flow rates this time was quite long and changes in the material could already have occurred during the wait period. Also, not all experiments were done at all temperatures and one material in one experiment had a different history than in the other. Therefore, the most comparable experiments are the ones performed at WHSV of 0.22 and 0.31 h^{-1}. Comparison of obtained concentrations of dibromomethane at both WHSVs (Figure 7b) and the temperatures at which the two flow rates were used show no similar trend. Comparison of bromine conversion calculated from concentrations of both products in both WHSVs and various temperatures is shown in Figure 8. At low temperatures, up to 340 °C, the conversion of bromine is slightly higher at a lower WHSV but at higher temperatures there is no significant difference between the two flow rates at the

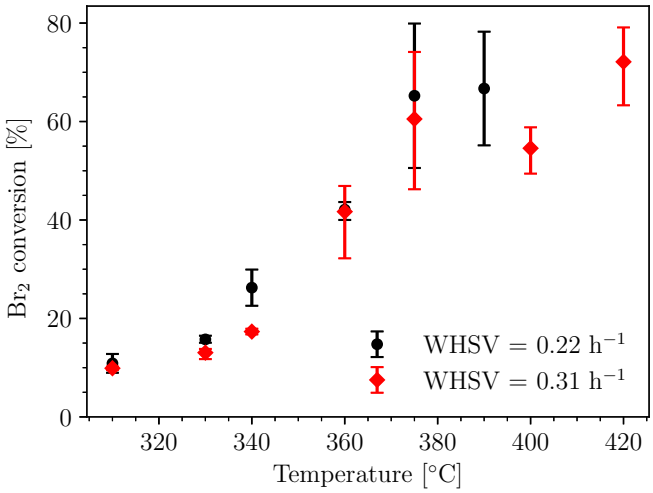

Figure 8: Conversion of Br_2 with temperature at two different WHSVs.

same loading of catalyst.

To determine whether the reason for the decrease in the concentration of dibromomethane at a temperature higher than 375 °C is its conversion to other products, additional experiments were performed with only dibromomethane reacting over SAPO-34. Here the carrier gas (He) carried dibromomethane vapours into a packed-bed reactor filled with 1 g of SAPO-34. Results are presented in Figure 9. Figure 9a shows the results of the reaction at 410 °C with WHSV of 0.42 h^{-1} and in Figure 9b the results at different temperatures and WHSV of 0.09 h^{-1} are presented. The results at 410 °C (Figure 9a) confirm that methyl bromide is formed from dibromomethane. This can also happen during the bromination of methane. Therefore, this could be a reason for the observed decrease in dibromomethane concentration at temperatures above 375 °C. The conversion of dibromomethane directly to methyl bromide is not possible due to stoichiometry. Most likely explanation is that dibromomethane decomposes on the surface of SAPO-34, where part of the carbon remains in the form of coke and methyl bromide and hydrogen bromide are released in the gas phase. The decomposition reaction of dibromomethane is most likely caused by acid sites on the catalyst similar to what happens in methanol to olefins reaction where Brønsted acid sites are responsible for activation, decomposition and recombination of methanol and hydrocarbons in methanol to hydrocarbons reaction and for coke formation [50, 51]. Bromine can be released from the surface of SAPO-34 in the form of methyl bromide or hydrogen bromide. With time on stream, the surface of the material becomes covered in coke and SAPO-34 is less active for decomposition of dibromomethane and methyl bromide concentration decreases and dibromomethane concentration increases with time on stream.

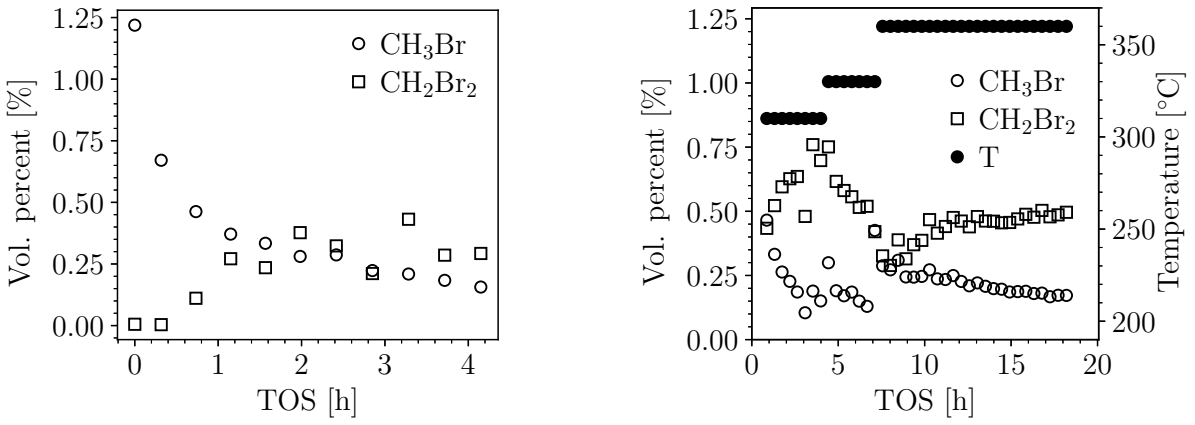

(a) Reaction conditions: WHSV = 0.42 h^{-1}, T = 410 °C, 2 vol.% CH_2Br_2 in He.

(b) Reaction conditions: WHSV = 0.09 h^{-1}, 1.6 vol.% CH_2Br_2 in He.

Figure 9: Decomposition of CH_2Br_2 over SAPO-34.

In the experiment, where the temperature was changed during the reaction in a stepwise manner (Figure 9b), the concentration of methyl bromide was decreasing with time on stream when the temperature was held constant. When the temperature was raised to 360 °C, the concentration of methyl bromide increased and then started to decrease. Dibromomethane was decomposing already at the lowest temperature (310 °C) where the concentration at the reactor outlet was below 1.6 vol.% which was present in the feed. Low concentrations of both dibromomethane and methyl bromide indicate that the majority of carbon from dibromomethane that was converted remained on the catalyst surface in the form of coke. After raising the temperature to 320 °C, the concentration of dibromomethane started to fall as the decomposition accelerated further. At the highest temperature (360 °C) the concentration first dropped somewhat due to more rapid decay on SAPO-34, but soon started to increase because the catalyst was being deactivated due to coke formation. Black coke was observed on the catalyst after both experiments. Photograph of the quartz reactor with SAPO-34 after reaction with CH_2Br_2 for 4.5 hours at 410 °C is shown in Figure S8 in Supplementary info. Part of the catalyst is also coloured orange, which might be a consequence of bromine formation and adsorption on the surface of the material. Similar orange colour was also observed on the SAPO-34 that was used for methane bromination (Figure S1). On both sides of the catalyst there is SiC.

Batamack et al. [37] reported that it is possible to obtain high selectivity for methyl bromide over SAPO-34 under appropriate methane bromination conditions. With a longer residence time (or smaller WHSV), the resulting methyl bromide combines to form ethylene and hydrogen bromide. At a shorter residence time 100% selectivity for methyl bromide was achieved at 365 °C. Different catalyst loadings were used to achieve

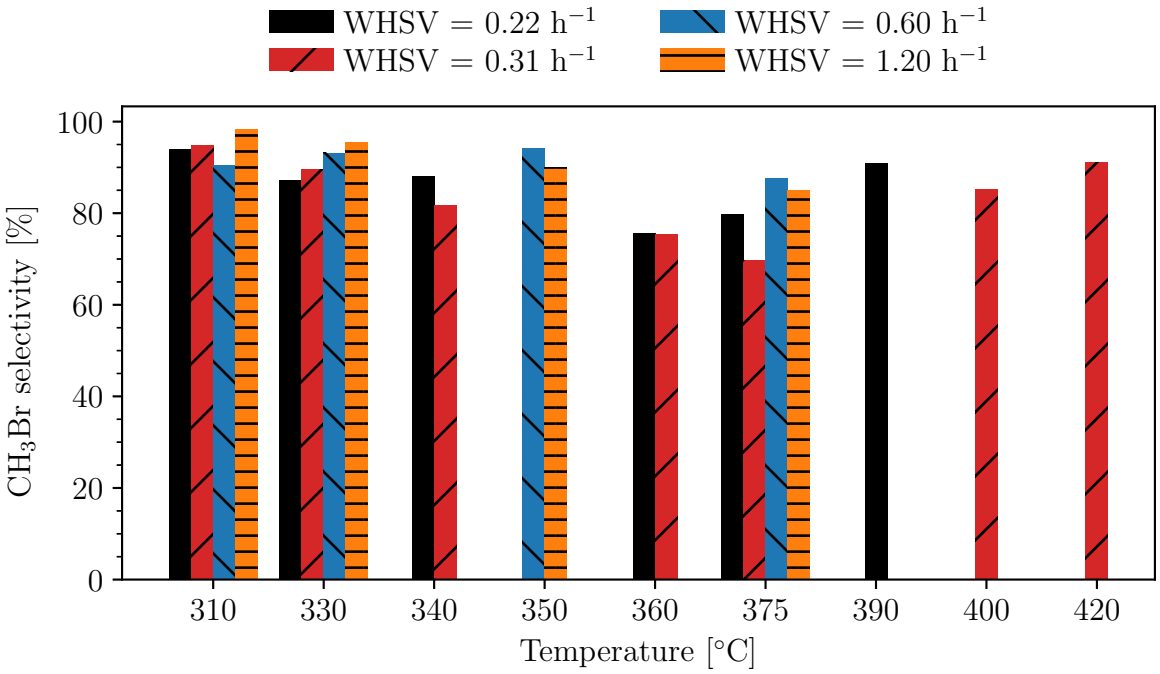

Figure 10: Selectivity for CH_3Br in methane bromination over SAPO-34.

different WHSV. At a smaller catalyst loading (1 g) the WHSV was 0.558 h^{-1} and at a larger catalyst loading (3 g) the WHSV was 0.186 h^{-1}. The content of Br_2 in the inlet mixture was 8.8 vol.% [37]. Similar conditions were applied in the present work for methane bromination reactions over SAPO-34. However, selectivity for methyl bromide never reached 100%. Obtained selectivities for methyl bromide under all experimental conditions of methane bromination with SAPO-34 are shown in Figure 10. Note that reaction was not performed for all 9 temperatures at all WHSVs. The reason for lower selectivity for methyl bromide could be a difference in material and experimental conditions. The selectivity for methyl bromide (S_{CH_3Br}) in Figure 10 was calculated by the equation 1.

$$S_{CH_3Br} = C_{CH_3Br}/(C_{CH_3Br} + C_{CH_2Br_2}) \tag{1}$$

The molar concentration of methyl bromide is C_{CH_3Br} and the molar concentration of dibromomethane is denoted by $C_{CH_2Br_2}$. No obvious trends with WHSV are observed in Figure 10. It should be noted that selectivity drops with temperature in the range between 360 °C and 375 °C, and then, at higher temperatures, begins to slightly rise again, as dibromomethane decomposes more rapidly on SAPO-34 to

form coke, methyl bromide and HBr. Bromination of methane in the gas phase shows a different trend for equilibrium methyl bromide selectivity with temperature. It is decreasing from 330 to 410 °C as shown in Figure S9. Equilibrium composition was calculated using Aspen Plus® V11. The decline in selectivity with temperature over SAPO-34 is the opposite of the selectivity predicted by the thermodynamic equilibrium. Therefore, the selectivity is controlled by the kinetics of methane bromination over SAPO-34. Reactions were performed at temperatures below 420 °C and at residence time shorter than 1 min, which means that they took place in the kinetic mode [31].

Paunović and Pérez-Ramírez [28] also did not observe an enhancement in the selectivity for methyl bromide when SAPO-34 was used. In that case the selectivity was around 80–85%, while in the empty reactor the selectivity was around 90%. They showed that methane bromination proceeds via a radical mechanism in the gas phase. Thus, SAPO-34 could increase the selectivity for methyl bromide only if its shape selectivity and confinement of radicals and reactants would facilitate formation of methyl bromide and suppress formation of polybrominated products. Similar confinement effect in high-silica zeolites was already thoroughly investigated in the case of NO oxidation [52, 53]. In the case of methane chlorination confinement of chlorine radical and methane in HZSM-5 increased conversion of methane but not selectivity to methyl chloride while in methane bromination over SAPO-34 no significant increase in conversion of methane compared to the empty reactor was observed [28].

Batamack et al. [37] proposed that bromine is activated on Brønsted acid sites of SAPO-34 resulting in formation of bromooxonium ion species which can subsequently react with methane to selectively form methyl bromide. For methane chlorination over zeolites (mordenite, X, Y, NaL and HZSM-5) it was shown that selectivity for methyl chloride was low at temperatures lower than 300 °C therefore radical mechanism is more probable, whereas at temperatures above 300–350 °C high selectivity for methyl chloride was achieved and mechanism involving acid sites was more probable [35]. According to Olah et al. [34], another type of active sites could also influence the activity and selectivity of the catalyst, namely Lewis acid sites present in SAPO-34 in the form of extra-framework aluminium which can be formed from reaction of SAPO-34 with hydrogen bromide and bromine during the methane bromination. On the contrary to these findings results presented herein and work of Paunović and Pérez-Ramírez [28] indicate that 100% selectivity for methyl bromide is difficult to achieve on SAPO-34 and thus radical mechanism in the gas phase is more probable. Although strong BAS in supported acid catalysts were already identified to be active sites for selective chlorination an bromination of methane by Olah et al. [34], results presented herein indicate that BAS in SAPO-34 do not play a role.

4. Conclusions

Bromination of methane could be a suitable way of methane valorization with a subsequent coupling of methyl bromide to ethylene. In this approach a high selectivity (approaching 100%) for methyl bromide in methane bromination step is desired. In this work SAPO-34 with SiO_2/Al_2O_3 ratio of 0.5 was used for bromination of methane in an attempt to increase the selectivity for methyl bromide. During the reaction the crystallinity of SAPO-34 was decreasing due to reaction with Br_2 and HBr and dealumination. This caused changes in the acidity of the material. Density of Brønsted acid sites decreased and the density of Lewis acid sites increased after the reaction but this does not seem to have an effect on the reaction. Brønsted acid sites could play a role in the catalytic reaction however, the reactants underwent radical reaction rather than the catalytic one. Although a significant decrease in crystallinity was observed, the particles preserved their shape as seen under the scanning electron microscope. Also, a decrease in surface area was observed possibly due to the collapse of pores or the blockage of pores by the extra-framework aluminium. Bromine was also detected on the material in SEM-EDX confirming incorporation of Br in the material and breakage of Al(OH)Si bonds. In the catalytic reactions no significant effect of WHSV was observed in the range of experimental conditions. The highest selectivity for methyl bromide was observed at 310 °C. At this temperature and WHSV of 1.2 h^{-1} the selectivity was around 98 % at all the other conditions it was lower. Therefore, SAPO-34 did not improve the selectivity compared to the gas phase bromination of methane and also the enhancement of the selectivity through confinement effect was not observed. Selectivity for methyl bromide was somewhat decreasing with increasing the temperature but above 360 °C it started to increase again because dibromomethane started to decompose on SAPO-34 at those temperatures. This was confirmed in the experiment where only dibromomethane was fed into the reactor filled with SAPO-34. It was found that dibromomethane decomposes on SAPO-34 to coke, methyl bromide and HBr already at 310 °C but more rapidly at higher temperatures. In methane bromination reaction coke was also being deposited at temperatures above 375 °C as a result of dibromomethane decomposition. In fact the largest amount of dibromomethane was forming at 375 °C and above this temperature a significant decrease in dibromomethane concentration at the reactor outlet was observed. Therefore, the results suggest that a possible enhancement of selectivity for methyl bromide could come only from decomposition of dibromomethane on SAPO-34 which is not advantageous compared to the gas phase bromination. In short the main findings are that during bromination of methane over SAPO-34 dealumination happens, bromine is being incorporated into the framework of material, coke deposition can happen at temperatures higher than 375 °C due to decomposition of formed products, mostly dibromomethane which can increase selectivity to

methyl bromide because it is a decomposition product.

Acknowledgements

Authors would like to thank Anže Prašnikar for providing SEM images, Urška Kavčič for performing N_2 physisorption and Edi Kranjc for XRD measurements. Janvit Teržan is acknowledged for the help with TPD analysis. This work was supported by Slovenian Research Agency (ARRS) through the following funding: core funding programme P2-0152, young researchers programme and project J2-1724.

References

[1] B. Dudley, et al., BP statistical review of world energy 2019, BP Statistical Review, London 1 (2019) 30–41.

[2] K. A. Willyard, A license to pollute? Opportunities, incentives, and influences on oil and gas venting and flaring in Texas, Energy Research & Social Science 62 (2020) 101381.

[3] B. Buzcu-Guven, R. Harriss, Extent, impacts and remedies of global gas flaring and venting, Carbon Management 3 (2012) 95–108.

[4] Analysis and forecasts to 2023, 2018. URL: `https://www.iea.org/gas2018/`.

[5] S. Faramawy, T. Zaki, A.-E. Sakr, Natural gas origin, composition, and processing: A review, Journal of Natural Gas Science and Engineering 34 (2016) 34–54.

[6] H. Zhang, Z. Sun, Y. H. Hu, Steam reforming of methane: Current states of catalyst design and process upgrading, Renewable and Sustainable Energy Reviews 149 (2021) 111330.

[7] A. Salcedo, P. G. Lustemberg, N. Rui, R. M. Palomino, Z. Liu, S. Nemsak, S. D. Senanayake, J. A. Rodriguez, M. V. Ganduglia-Pirovano, B. Irigoyen, Reaction Pathway for Coke-Free Methane Steam Reforming on a Ni/CeO_2 Catalyst: Active Sites and the Role of Metal–Support Interactions, ACS catalysis 11 (2021) 8327–8337.

[8] S. A. Shin, Y. S. Noh, G. H. Hong, J. I. Park, H. T. Song, K.-Y. Lee, D. J. Moon, Dry reforming of methane over Ni/ZrO_2-Al_2O_3 catalysts: Effect of preparation methods, Journal of the Taiwan Institute of Chemical Engineers 90 (2018) 25–32.

[9] M. R. Shamsuddin, N. Asikin-Mijan, M. I. Saiman, T. S. Marliza, M. A. Yarmo, Y. H. Taufiq-Yap, Evaluation of NiO/TALC Catalytic performance in carbon dioxide reforming of methane, Journal of the Taiwan Institute of Chemical Engineers 122 (2021) 106–117.

[10] A. Mosayebi, Kinetic modeling of catalytic partial oxidation of methane over Ni-Rh/γ-Al_2O_3 catalyst for syngas formation, Journal of the Taiwan Institute of Chemical Engineers 114 (2020) 36–46.

[11] J. Shakeri, M. Joshaghani, H. Hadadzadeh, M. J. Shaterzadeh, Methane carbonylation to light olefins and alcohols over carbon–based iron–and cobalt–oxide catalysts, Journal of the Taiwan Institute of Chemical Engineers 122 (2021) 127–135.

[12] U. S. Mohanty, M. Ali, M. R. Azhar, A. Al-Yaseri, A. Keshavarz, S. Iglauer, Current advances in syngas (CO + H_2) production through bi-reforming of methane using various catalysts: A review, International Journal of Hydrogen Energy 46 (2021) 32809–32845.

[13] D. P. Minh, X.-H. Pham, T. J. Siang, D.-V. N. Vo, Review on the catalytic tri-reforming of methane-Part I: Impact of operating conditions, catalyst deactivation and regeneration, Applied Catalysis A: General 621 (2021) 118202.

[14] D. A. Wood, C. Nwaoha, B. F. Towler, Gas-to-liquids (GTL): A review of an industry offering several routes for monetizing natural gas, Journal of Natural Gas Science and Engineering 9 (2012) 196–208.

[15] A. I. Olivos-Suarez, A. Szécsényi, E. J. M. Hensen, J. Ruiz-Martinez, E. A. Pidko, J. Gascon, Strategies for the direct catalytic valorization of methane using heterogeneous catalysis: challenges and opportunities, Acs Catalysis 6 (2016) 2965–2981.

[16] U. Zavyalova, M. Holena, R. Schlögl, M. Baerns, Statistical analysis of past catalytic data on oxidative methane coupling for new insights into the composition of high-performance catalysts, ChemCatChem 3 (2011) 1935–1947.

[17] J. Xu, Y. Zhang, X. Xu, X. Fang, R. Xi, Y. Liu, R. Zheng, X. Wang, Constructing La2B2O7 (B = Ti, Zr, Ce) compounds with three typical crystalline phases for the oxidative coupling of methane: the effect of phase structures, superoxide anions, and alkalinity on the reactivity, ACS Catalysis 9 (2019) 4030–4045.

[18] J. Xu, Y. Zhang, Y. Liu, X. Fang, X. Xu, W. Liu, R. Zheng, X. Wang, Optimizing the Reaction Performance of La2Ce2O7-Based Catalysts for Oxidative Coupling of Methane (OCM) at Lower Temperature by Lattice Doping with Ca Cations, European Journal of Inorganic Chemistry 2019 (2019) 183–194.

[19] K. Sun, D. M. Ginosar, T. He, Y. Zhang, M. Fan, R. Chen, Progress in nonoxidative dehydroaromatization of methane in the last 6 years, Industrial & Engineering Chemistry Research 57 (2018) 1768–1789.

[20] X. Guo, G. Fang, G. Li, H. Ma, H. Fan, L. Yu, C. Ma, X. Wu, D. Deng, M. Wei, et al., Direct, nonoxidative conversion of methane to ethylene, aromatics, and hydrogen, Science 344 (2014) 616–619.

[21] S. J. Han, S. W. Lee, H. W. Kim, S. K. Kim, Y. T. Kim, Nonoxidative Direct Conversion of Methane on Silica-Based Iron Catalysts: Effect of Catalytic Surface, ACS Catalysis 9 (2019) 7984–7997.

[22] K. Dutta, V. Chaudhari, C.-J. Li, J. Kopyscinski, Methane conversion to ethylene over GaN catalysts. Effect of catalyst nitridation, Applied Catalysis A: General (2020) 117430.

[23] P. Xie, T. Pu, A. Nie, S. Hwang, S. C. Purdy, W. Yu, D. Su, J. T. Miller, C. Wang, Nanoceria-supported single-atom platinum catalysts for direct methane conversion, ACS Catalysis 8 (2018) 4044–4048.

[24] Y. Xiao, A. Varma, Highly selective nonoxidative coupling of methane over Pt-Bi bimetallic catalysts, ACS Catalysis 8 (2018) 2735–2740.

[25] M. Peter, T. J. Marks, Platinum Metal-Free Catalysts for Selective Soft Oxidative Methane to Ethylene Coupling. Scope and Mechanistic Observations, Journal of the American Chemical Society 137 (2015) 15234–15240.

[26] Q. Zhu, S. L. Wegener, C. Xie, O. Uche, M. Neurock, T. J. Marks, Sulfur as a selective 'soft'oxidant for catalytic methane conversion probed by experiment and theory, Nature chemistry 5 (2013) 104–109.

[27] S. Kwon, H.-J. Chae, K. Na, Control of methane chlorination with molecular chlorine gas using zeolite catalysts: Effects of Si/Al ratio and framework type, Catalysis Today (2020).

[28] V. Paunović, J. Pérez-Ramírez, Catalytic halogenation of methane: a dream reaction with practical scope?, Catalysis Science & Technology 9 (2019) 4515–4530.

[29] K. Ding, H. Metiu, G. D. Stucky, The selective high-yield conversion of methane using iodine-catalyzed methane bromination, ACS Catalysis 3 (2013) 474–477.

[30] G. Kistiakowsky, E. Van Artsdalen, Bromination of Hydrocarbons. I. Photochemical and Thermal Bromination of Methane and Methyl Bromine. Carbon-Hydrogen Bond Strength in Methane, The Journal of Chemical Physics 12 (1944) 469–478.

[31] I. M. Lorkovic, S. Sun, S. Gadewar, A. Breed, G. S. Macala, A. Sardar, S. E. Cross, J. H. Sherman, G. D. Stucky, P. C. Ford, Alkane bromination revisited:"reproportionation" in gas-phase methane bromination leads to higher selectivity for CH_3Br at moderate temperatures, The Journal of Physical Chemistry A 110 (2006) 8695–8700.

[32] A. Zhang, S. Sun, Z. J. Komon, N. Osterwalder, S. Gadewar, P. Stoimenov, D. J. Auerbach, G. D. Stucky, E. W. McFarland, Improved light olefin yield from methyl bromide coupling over modified SAPO-34 molecular sieves, Physical Chemistry Chemical Physics 13 (2011) 2550–2555.

[33] S. Svelle, S. Aravinthan, M. Bjørgen, K.-P. Lillerud, S. Kolboe, I. M. Dahl, U. Olsbye, The methyl halide to hydrocarbon reaction over H-SAPO-34, Journal of Catalysis 241 (2006) 243–254.

[34] G. A. Olah, B. Gupta, J. D. Felberg, W. M. Ip, A. Husain, R. Karpeles, K. Lammertsma, A. K. Melhotra, N. J. a. Trivedi, Electrophilic reactions at single bonds. 20. Selective monohalogenation of methane over supported acidic or platinum metal catalysts and hydrolysis of methyl halides over .gamma.-alumina-supported metal oxide/hydroxide catalysts. A feasible path for the oxidative conversion of methane into methyl alcohol/dimethyl ether, Journal of the American Chemical

Society 107 (1985) 7097–7105.

[35] I. Bucsi, G. A. Olah, Selective monochlorination of methane over solid acid and zeolite catalysts, Catalysis letters 16 (1992) 27–38.

[36] V. Degirmenci, A. Yilmaz, D. Uner, Selective methane bromination over sulfated zirconia in SBA-15 catalysts, Catalysis Today 142 (2009) 30–33.

[37] P. T. Batamack, T. Mathew, G. S. Prakash, One-Pot Conversion of Methane to Light Olefins or Higher Hydrocarbons through H-SAPO-34-Catalyzed in Situ Halogenation, Journal of the American Chemical Society 139 (2017) 18078–18083.

[38] S. Brunauer, P. H. Emmett, E. Teller, Adsorption of gases in multimolecular layers, Journal of the American chemical society 60 (1938) 309–319.

[39] J. H. De Boer, B. C. Lippens, B. G. Linsen, J. C. P. Broekhoff, A. Van den Heuvel, T. J. Osinga, The t-curve of multimolecular N_2-adsorption, Journal of Colloid and Interface Science 21 (1966) 405–414.

[40] H. Yang, Z. Liu, H. Gao, Z. Xie, Synthesis and catalytic performances of hierarchical SAPO-34 monolith, Journal of Materials Chemistry 20 (2010) 3227–3231.

[41] R. Iwanowski, K. Fronc, W. Paszkowicz, M. Heinonen, XPS and XRD study of crystalline 3C-SiC grown by sublimation method, Journal of alloys and compounds 286 (1999) 143–147.

[42] V. Paunović, S. Mitchell, R. Verel, S. S. Lee, J. Pérez-Ramírez, Aluminum Redistribution in ZSM-5 Zeolite upon Interaction with Gaseous Halogens and Hydrogen Halides and Implications in Catalysis, The Journal of Physical Chemistry C 124 (2019) 722–733.

[43] Y. Wei, D. Zhang, Z. Liu, B.-L. Su, Highly efficient catalytic conversion of chloromethane to light olefins over HSAPO-34 as studied by catalytic testing and in situ FTIR, Journal of Catalysis 238 (2006) 46–57.

[44] P. Tian, G. Zhan, J. Tian, K. B. Tan, M. Guo, Y. Han, T. Fu, J. Huang, Q. Li, Direct co2 hydrogenation to light olefins over znzrox mixed with hierarchically hollow sapo-34 with rice husk as green silicon source and template, Applied Catalysis B: Environmental (2022) 121572.

[45] C. Wang, M. Yang, P. Tian, S. Xu, Y. Yang, D. Wang, Y. Yuan, Z. Liu, Dual template-directed synthesis of sapo-34 nanosheet assemblies with improved stability in the methanol to olefins reaction, Journal of Materials Chemistry A 3 (2015) 5608–5616.

[46] G. Martins, G. Berlier, C. Bisio, S. Coluccia, H. Pastore, L. Marchese, Quantification of Brønsted acid sites in microporous catalysts by a combined FTIR and NH_3-TPD study, The Journal of Physical Chemistry C 112 (2008) 7193–7200.

[47] D. Wang, L. Zhang, J. Li, K. Kamasamudram, W. S. Epling, NH_3-SCR over Cu/SAPO-34–Zeolite acidity and Cu structure changes as a function of Cu loading, Catalysis Today 231 (2014) 64–74.

[48] M. Thommes, K. Kaneko, A. V. Neimark, J. P. Olivier, F. Rodriguez-Reinoso, J. Rouquerol, K. S. Sing, Physisorption of gases, with special reference to the evaluation of surface area and pore size distribution (IUPAC Technical Report), Pure and Applied Chemistry 87 (2015) 1051–1069.

[49] J. Zheng, J. Ding, D. Jin, G. Ye, K. Zhu, X. Zhou, W. Yang, W. Yuan, The tailored synthesis of nanosized SAPO-34 via time-controlled silicon release enabled by an organosilane precursor, Chemical Communications 53 (2017) 6132–6135.

[50] J. E. Schmidt, J. D. Poplawsky, B. Mazumder, Ö. Attila, D. Fu, D. M. de Winter, F. Meirer, S. R. Bare, B. M. Weckhuysen, Coke Formation in a Zeolite Crystal During the Methanol-to-Hydrocarbons Reaction as Studied with Atom Probe Tomography, Angewandte Chemie International Edition 55 (2016) 11173–11177.

[51] W. Dai, X. Wang, G. Wu, N. Guan, M. Hunger, L. Li, Methanol-to-olefin conversion on silicoaluminophosphate catalysts:

Effect of Brønsted acid sites and framework structures, ACS catalysis 1 (2011) 292–299.

[52] N. Artioli, R. F. Lobo, E. Iglesia, Catalysis by confinement: Enthalpic stabilization of no oxidation transition states by microporororous and mesoporous siliceous materials, The Journal of Physical Chemistry C 117 (2013) 20666–20674.

[53] M. Maestri, E. Iglesia, First-principles theoretical assessment of catalysis by confinement: NO–O_2 reactions within voids of molecular dimensions in siliceous crystalline frameworks, Physical Chemistry Chemical Physics 20 (2018) 15725–15735.